BRICS TRANSPORT
VOL. 1 ISSUE 1 2022
TRANSPORT ECOSYSTEM: SOCIETY, STATE, AND GLOBAL CHALLENGES
ЭКОСИСТЕМА ТРАНСПОРТА: ОБЩЕСТВО, ГОСУДАРСТВО И ГЛОБАЛЬНЫЕ ВЫЗОВЫ

Original article
UDC 621.311
doi:10.46684/2022.1.1

Innovative energy sources for Hyperloop high-speed transport

Konstantin K. Kim[1]✉, Alexander Yu. Panychev[2], Lyudmila S. Blazhko[3]

[1, 2, 3] Emperor Alexander I St. Petersburg State Transport University (PGUPS); St. Petersburg, Russian Federation

[1] kimkk@inbox.ru✉; https://orcid.org/0000-0001-7282-4429

[2] dou@pgups.ru; https://orcid.org/0000-0003-1859-3097

[3] blazhko@pgups.ru; https://orcid.org/0000-0001-5209-6778

ABSTRACT This article describes an innovative design of a solar-wind generator for a distributed energy Hyperloop high-speed system. The knowhow of this development is to mount flexible silicon solar panels (SP) on wind turbine blades, thus optimizing the thermal efficiency of solar panels. The basic dimensions of the wind turbine blades and the maximum internal flow velocities at the blade outlet (tips) are presented. At low wind velocities, it is rational to locate solar panels on the outer end (or the tip) of a blade, rather than along the blade length.

The cooling effect can be increased by using materials with low thermal resistance for the SP and blades, or by reducing their thickness.

To increase the heat transfer coefficient, it is recommended to use the airflow turbulence on the solar panel surface. In practice, this can be achieved both by changing the operating parameters and by introducing innovative design solutions.

For better cooling of solar panels, it is recommended to use the technology of a wind flow sucked into the blade inner cavity.

Changing the geometry of the outer end (tip) of the blades and the use of deflectors also give a better panel cooling parameters.

KEYWORDS: hyperloop high-speed transport; solar-turbine generator; flexible silicon solar panel; solar insolation; wind flow; heat transfer coefficient; temperature; blade inner cavity

For citation: Kim K.K., Panychev A.Yu., Blazhko L.S. Innovative energy sources for Hyperloop high-speed transport. *BRICS transport*. 2022;1(1):1. https://doi.org/10.46684/2022.1.1

Научная статья

Использование инновационных альтернативных источников энергии в трубопроводном высокоскоростном транспорте

К.К. Ким[1]✉, А.Ю. Панычев[2], Л.С. Блажко[3]

[1, 2, 3] Петербургский государственный университет путей сообщения Императора Александра I (ПГУПС); г. Санкт-Петербург, Россия

[1] kimkk@inbox.ru✉; https://orcid.org/0000-0001-7282-4429

[2] dou@pgups.ru; https://orcid.org/0000-0003-1859-3097

[3] blazhko@pgups.ru; https://orcid.org/0000-0001-5209-6778

АННОТАЦИЯ Рассматривается инновационная конструкция гелиоветрогенератора, предназначенная для распределенной системы электроснабжения трубопроводного высокоскоростного транспорта. Know how данной разработки заключается в закреплении гибких кремниевых солнечных панелей (СП) на лопастях ветротурбины. За счет этого возможно обеспечение оптимального теплового режима работы СП. Приводятся основные размеры конструкций лопасти и максимальные скорости внутреннего потока на выходе из лопасти. Показывается, что при малых скоростях ветрового потока рационально располагать СП не по всей площади лопасти, а ближе к ее концу.

Усиления эффекта охлаждения можно достичь, применяя материалы для СП и лопастей с малым полным термическим сопротивлением или уменьшая их толщину.

Для увеличения коэффициента теплоотдачи следует реализовывать турбулентный режим течения воздушного потока на поверхности СП. На практике это достигается как за счет изменения режимных параметров, так и с помощью конструктивных решений.

С целью усиления охлаждения панелей необходимо использовать часть ветрового потока, принудительно засасываемого во внутреннюю полость лопасти.

Изменение геометрии оконечных частей лопастей и применение дефлекторов также благоприятно сказываются на интенсивности охлаждения панелей.

КЛЮЧЕВЫЕ СЛОВА: трубопроводный высокоскоростной транспорт; гелиоветрогенератор; гибкая кремниевая солнечная панель; солнечная инсоляция; ветровой поток; коэффициент теплоотдачи; температура; внутренняя полость лопасти

Для цитирования: *Ким К.К., Панычев А.Ю., Блажко Л.С.* Использование инновационных альтернативных источников энергии в трубопроводном высокоскоростном транспорте // Транспорт БРИКС. 2022. Т. 1. Вып. 1. Ст. 1. https://doi.org/10.46684/2022.1.1.

INTRODUCTION

It is well-known that the advantages of Hyperloop high-speed transport are fully manifested on main lines (at longer distances and with fewer stops). It will be most efficient in a Hyperloop with low-pressure environment inside the tube (the air density is 1.5–2 times lower in comparison with that outside), with passenger capsules (pods) moving at a speed of 500–1000 km/h due to low aerodynamic resistance [1]. This technical solution will make it possible to reduce energy use required for a linear electric drive motor, which is particularly suitable in specific operating conditions. High speeds dictate the replacement of the "rail-wheel" mechanical system by Hyperloop capsules moving in a near-vacuum tube created by electromagnetic force [2].

When the capsule moves along the tube, a boundary air layer is created on its surface. Due to the capsule surface roughness, uneven airflow, capsule vibrations, etc., perturbations of the boundary air layer occur resulting in the turbulent spots that induce a turbulent state of almost the entire boundary air layer over time, thus, increasing sharply the aerodynamic drag of the capsule. To eliminate this and partially reduce the "piston" effect, the engineers of Emperor Alexander I St. Petersburg State Transport University (PGUPS) have put forward an idea of the perforated front surface of the capsule [3]. The incipient turbulent air is sucked through the holes of the perforated shell (*Fig. 1*) and the boundary layer maintains laminar character. This can result in up to 30 % lower frontal aerodynamic drag. At the same time, pressure equalization at the head and tail of the moving capsule (so-called "piston" effect) takes place. The airflow passing through the perforated holes is used for air conditioning and ventilation inside the capsule as well as cooling of the onboard current-carrying elements. Pumps can be used to produce turbulent air suction.

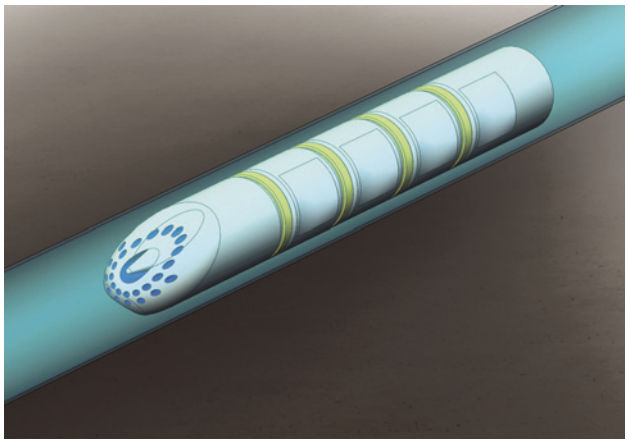

Fig. 1. Passenger capsule with the perforated front

A linear induction motor distributed along the inside wall of the tube is one of the main elements of this transport system. To reduce electric energy losses, energy sources should be distributed along the length of the tube, with each source responsible for their "own" section, electrically independent from the adjacent sections. Each energy source should switch on as soon as the capsule enters the corresponding section.

For energy sources, it is proposed to use solar-wind generators developed at the Electrical Engineering and Heat Engineering department (PGUPS, St. Petersburg, Russia) [4].

The know-how is as follows. Commonly used silicon solar panels have an inherent disadvantage: their efficiency decreases as their temperature exceeds a certain optimal value (about 25 °C) [5]. Thus, it is recommended to cool the solar panel by an incoming airflow. For this purpose, thin-film solar panels (SP) should be mounted on the wind turbine blades.

DESIGN

A horizontal axis wind turbine with three blades is taken as a basis for a solar-wind generator. Two developments have been considered. The first one is based on the AAERA 1500-70 turbine while the second one is based on the Micon 450/530 turbine (*Table 1*). E-Power flexible solar panels (*Table 2*) with Solar Sity photovoltaic cells are used. Solar panels *1* (*Fig. 2*) are attached to the blade *2* front surface. When sunlight hits the solar panels, they generate electric current according to the photovoltaic effect. Through a sliding current collector (not shown in the Figure), this current goes to a storage

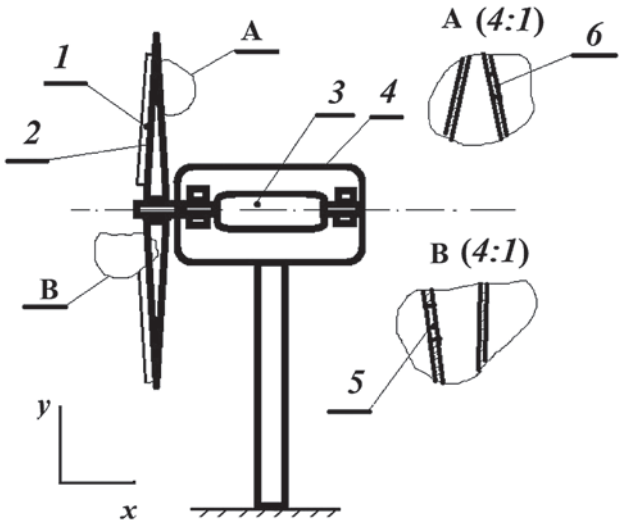

Fig. 2. Design of a solar-wind generator:
1 — solar panels; *2* — blades; *3* — cylindrical rotor; *4* — electric generator; *5*, *6* — holes

Table 1

Wind turbine characteristics

Parameters	AAERA 1500-70	Micon 450/530
Rated power, kW	1500	250
Minimum wind velocity at the beginning of operation, m/s	3	4.5
Rated wind speed, m/s	11.8	14.5
Maximum wind speed, m/s	59	50
Rotor diameter, m	77	26
Specific power, W/m^2	390	471.7
Generator	Asynchronous double-phase	Asynchronous three-phase
Voltage, V	480	400
Frequency	60 Hz	50 Hz

Table 2

E-Power 160 solar panel characteristics

Type	Monocrystalline
Number of cells in the module, pcs.	36
Cell size, mm	156 × 156
Power, W	160
Noload voltage, V	21.6
Operating voltage, V	18
Short-circuit current, A	9.07
Operating current, A	8.89
Cell efficiency, %	20

device (e.g. battery) located at the wind turbine tower base, or, in case of a synchronous generator, to the excitation winding (in this case, the sliding current collector is not used).

The rotation of the blades *2* starts the effective cooling of solar panel *1*. At the same time, the cylindrical rotor *3* of the electric generator *4* rotates; thus, the rotor kinetic energy is converted into electrical energy. It is possible to use electric generators of different types.

HEAT TRANSFER NUMERICAL SIMULATION FOR THE SOLAR-WIND GENERATOR BLADE

To determine the solar-wind turbine performance, the climate conditions with wind speed of 4.2 m/s, solar insolation of 5.79 kW/m^2 and ambient air temperature of 23.8 °C were chosen.

The rotor speed of the solar-wind turbine was ~5.

The solar heat absorbing surface area of three blades (assuming the blades had a rectangular shape) was 427.35 m^2 for AAERA 1500–70 and 49.14 m^2 for 450/530 Micon. The flexible solar cells were assumed to cover the entire surface of the blades. Ambient temperature over the course of a day could be modeled as a sinusoidal function according to the law:

$$T_{air}(t) = \Theta_{avg} + \Delta\Theta \cos\left(2\pi \frac{t-14}{24}\right), \quad (1)$$

where t is time, h; Θ_{avg} and $\Delta\Theta$ are adjustable parameters corresponding to the average temperature and temperature changes respectively during the day and night.

The calculations for Θ_{avg} = 22 °C and $\Delta\Theta$ =10 °C are shown in *Fig. 3*.

In the first part of simulation tests, three rotating blades we presented by a flat rotating disc of homogeneous thickness with a diameter equal to the diameter of the wind turbine rotor. The disc was made of fiberglass reinforced epoxy resin. The rotating speed of the disc was constant and equaled 5.2 rpm. Solar heating and convective heat transfer took place only at the front surface of the blades positioned perpendicular to the solar flux. The back and side surfaces of the disc were thermally insulated.

Temperature distributions along the disc radius for AAERA 1500-70 are shown in *Fig. 4*. Curve *1* corresponds to 6 o'clock, curve *2* to 8 o'clock, curve *3* to 10 o'clock, and curve *4* to 13.5 o'clock (time of maximum temperatures).

As seen from *Fig. 4*, the disc temperatures could be considered acceptable only in the early morning hours. Later in the day, the temperature exceeded its optimal value (25 °C). This fact should not be given much consideration because the equal size of the disc diameter and the wind turbine rotor diameter was of oversim-

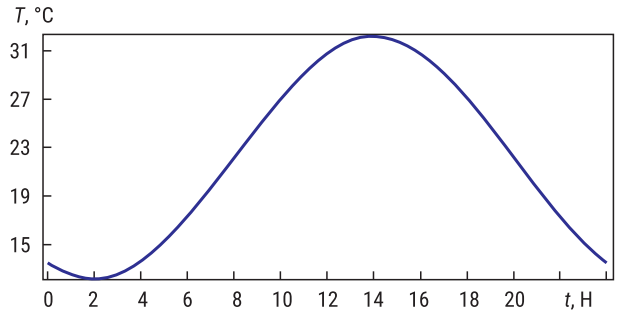

Fig. 3. Daily variations in ambient air temperature

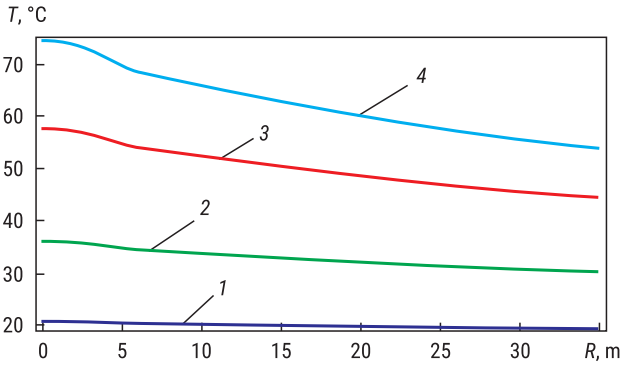

Fig. 4. Temperature distribution along the disk radius

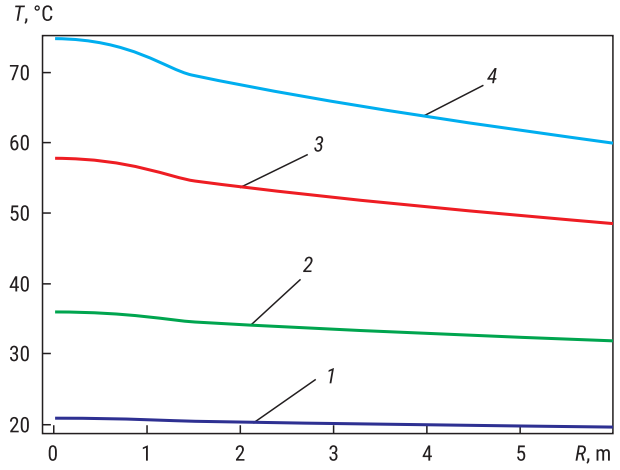

Fig. 5. Temperature distribution along the radius of the equivalent disc

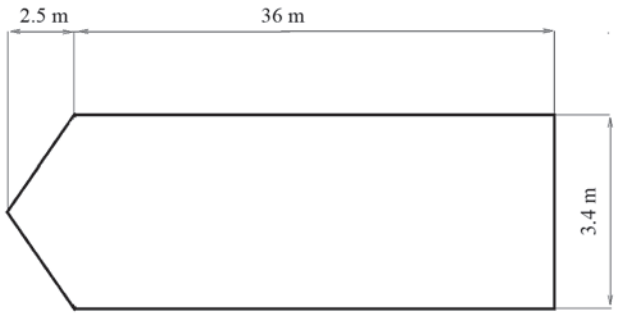

Fig. 6. Blade shape and dimensions

plified assumption. It is interesting to note that the received dependences illustrated the influence of the centrifugal force on the temperature distribution along the disc radius. The temperature decreased steadily towards the disc periphery.

At the second stage of the simulation, the three blades real area was taken into consideration, which was 427.35 m^2 for AAERA 1500-70. The diameter of the equivalent disk, in terms of the area exposed to solar insolation, was equal to 11.67 m.

The calculations are shown in *Fig. 5*. The dependence numbers correspond to the time points as in *Fig. 4*.

It should be noted that despite a certain temperature excess associated with the reduction of the heat transfer area, the conclusions for the 77 m diameter disc apply to this case as well.

The next issue to be considered was how much the real blade rotation will decrease the solar panel temperature. A blade shown in *Fig. 6* was taken as a model. The blade was assumed to be monolithic made of fiberglass reinforced epoxy resin.

The calculation was based on the heat transfer formula

$$\rho C_p \frac{\partial T}{\partial t} + \rho C_p u \nabla T + \nabla q = Q + Q_{ted}; \quad (2)$$

$$q = -k\nabla T, \quad (3)$$

where ρ is the density; C_p is the specific heat capacity; the change of temperature field over a period of time; $\partial T/\partial t$ is the temperature field gradient; q is the density of the heat flow transferred from the surface to the environment; Q is the heat flow; $-k$ is the heat transfer coefficient. The minus sign shows that the heat flows in the opposite to the vector direction.

However, even in this case, the blade front surface temperatures reached 140 °C, which can be explained by a very low thermal conductivity of the blade material. Therefore, an additional summand Q_{ted} was introduced to change the external heat flow.

The time dependences of the solar heat flow and the ambient air temperature were the same as those for the disc.

The symmetry condition $-nq = 0$ was set on two blade surfaces located at an acute angle (*Fig. 6*). The other surfaces were thermally insulated, which suited the symmetry condition in appearance.

The dependences in *Fig. 7* show the temperature distribution along the longitudinal axis of the blade at different values of the heat transfer coefficient: curve *1* corresponds to 5 W/(m^2 · K), curve *2* to 10 W/(m^2 · K), and curve *3* to 15.5 W/(m^2 · K).

Fig. 8 shows temperature distributions along the longitudinal axis of the blade of Micon 450/530 wind turbine at different times of the day for the heat transfer coefficient equal to 10 W/(m^2 · K) and 15.5 W/m^2 · K respectively. The length of the blade is 13 m; the width

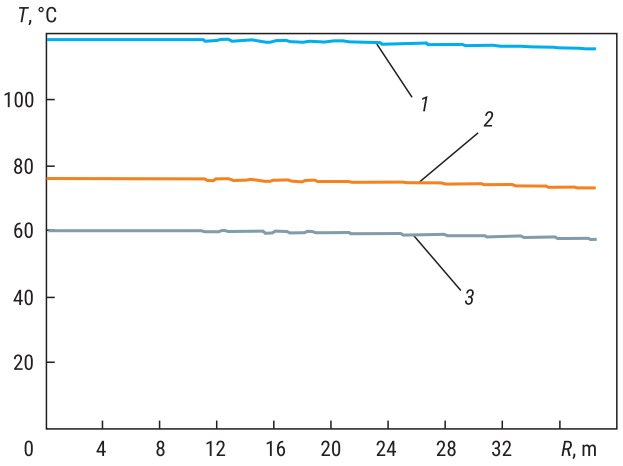

Fig. 7. Graphs of temperature distribution for different heat transfer coefficients ($2R$ = 77 m)

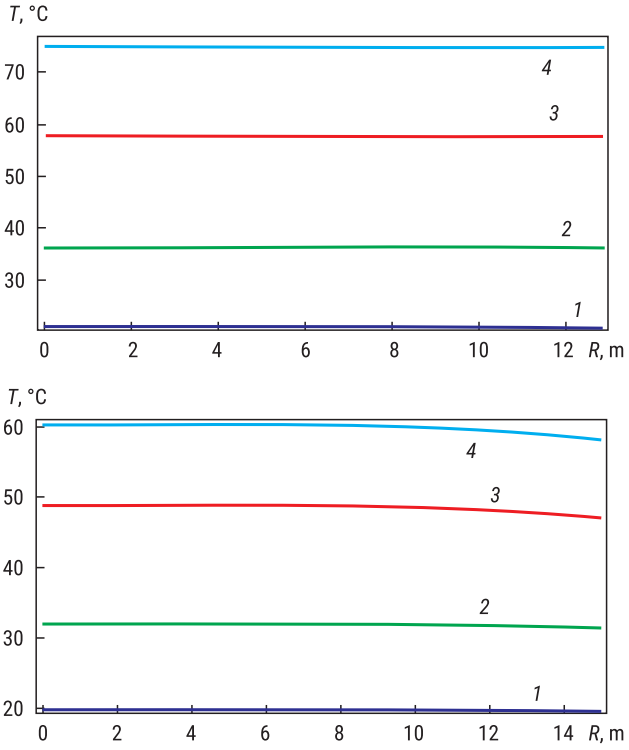

Fig. 8. Graphs of temperature distribution along the longitudinal axis of Micon 450/530 wind turbine blade at different times of the day

is 2.2 m. Curve *1* corresponds to 6 o'clock, curve *2* to 8 o'clock, curve *3* to 10 o'clock, and curve *4* to 12 o'clock.

As was expected, the maximum blade (panel) temperatures were observed in the hours close to noon (*Fig. 9*).

Thus, under the assumed climatic conditions, this design solution, namely, the location of solar panels on the wind turbine blades, does not prove to be efficient for obtaining the optimal temperature of 25 °C, even if a certain temperature reduction was proved to take place. However, the results obtained in the course of simulations allowed making some preliminary conclusions and outlining further research fields.

The heat transfer coefficient can be improved by increasing the wind turbine rotational speed.

The airflow turbulence near the solar panel surface can improve its thermal condition. Turbulent air pulsations increase the panel heat transfer. In practice, the air turbulence can be achieved by changing the operating parameters or by new design solutions. For example, spiral grooves on the blade and solar panel surfaces or artificially created roughness of the solar panel surface can induce airflow perturbations. Aerodynamics and strength factors should be taken into consideration when studying the feasibility of these solutions.

The heating rate of the solar panel decreases towards the blade tip (see *Fig. 7*, *8*), so at low wind velocity, it is rational to place the solar panels closer to the turbine blade end (tip) rather than over its entire area.

The cooling effect can be improved by reducing the thermal resistance of solar panels in the direction perpendicular to their front surface. The use of materials with greater thermal transfer coefficient and thinner solar panels can improve the cooling effect.

INNOVATIVE DESIGN

A cooling mechanism of the blade front surface has been described above. Cooling the blade from inside seems significant as well (see *Fig. 2*). To make it possible, the blade should be hollow inside and have an inlet hole 5 at the rim (on the blade front surface) and an outlet hole 6 at the blade back surface tip (*Fig. 2*) [6].

The "sucking" of the airflow inside the blade occurs as follows. Approaching the sweeping area of the rotating blades (*Fig. 10*, *y*-axis), the wind flow slows down

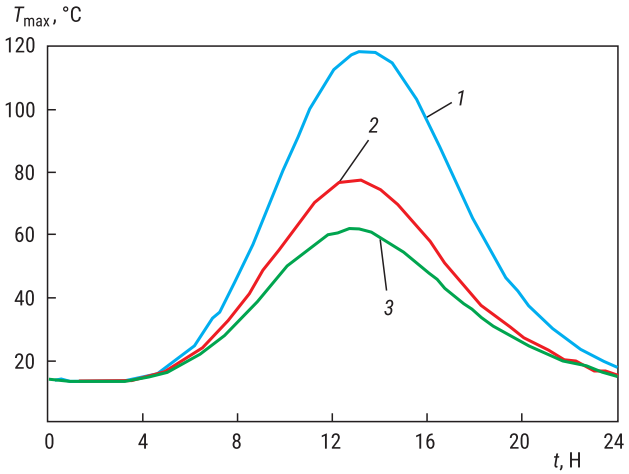

Fig. 9. Change of blade maximum temperatures during the day: curve *1* corresponds to 5 W/(m²·K); curve *2* to 10 W/(m²·K); curve *3* to 15.5 W/(m²·K)

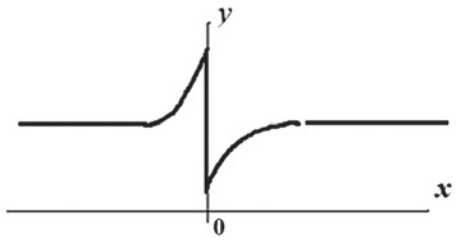

Fig. 10. Pressure diagram

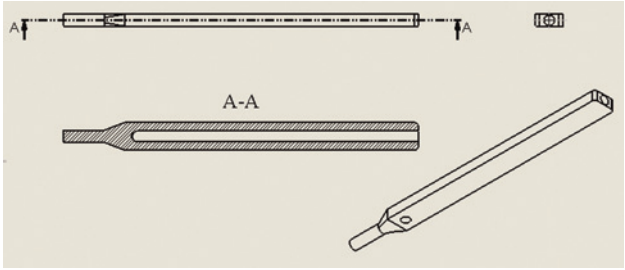

Fig. 11. Straight blade design

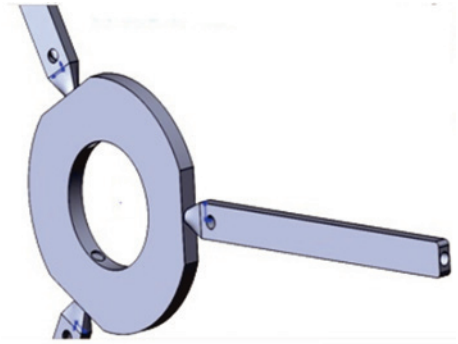

Fig. 12. Wind turbine rotor

and its speed decreases causing the static pressure increase in this area, according to Bernoulli's law. As the wind stream passes through the front area of rotating blades, it meets lower resistance and the air pressure drops suddenly. Because of this pressure drop, the air is partially sucked into hole *5* inside the blade (*Fig. 2*). Passing through the blade inner cavity, the air exits hole *6* (*Fig. 2*). As a result, the blade (panel) is cooled by the inside air.

SIMULATION OF A BLADE WITH AN INTERNAL CAVITY IN SOLIDWORKS

"Straight" blade design

The effect of blade rotation on the airflow velocity inside the blade was studied using SolidWorks.

For simplification, the turbine blade (multilayer heterogeneous structure) was represented as a rectangular hollow parallelepiped with a cylindrical rim. It was called a straight blade design (*Fig. 11*).

Fig. 12 shows a fragment of the wind turbine rotor.

The SolidWorksFlow simulation based on the Finite Volume Method was used to simulate wind flow through the blade inner cavity.

The boundary conditions were set by the "real moving wall" surface. The coordinate system was referenced to the rotor. The model rotated counterclockwise at an angular velocity of –2.62 rad/s.

The simulation analysis showed that with the wind velocity in front of the rotor being 4.2 m/s, the airflow inside the "straight" blade cavity had a velocity as low as 0.2 m/s and was turbulent in nature. This led to further improvement of the blade design.

A flanged blade tip design

The effect of a flanged blade tip on the internal airflow velocity was studied. The flanged tip consisted of a "knee" bend of a certain length attached to the blade tip at an angle relative to the longitudinal axis of the blade.

The basic dimensions of solar-wind generator blade designs under consideration are presented in *Table 3* (*L* is the length of the main part of the blade).

Table 3

Main dimensions of the turbine blade designs and maximum internal flow velocities at the blade output

Blade knee-bend length, % of *L*	Angle of the knee bend, deg.	Maximum airflow velocity at the blade output, m/s
5	90	0.83
10	90	1.20
15	90	1.43
20	90	1.45
5	30	0.70
10	30	1.10
15 The best option	**30**	**1.51**
20	30	1.45
5	–30	1.20
10	–30	1.27
15	–30	1,25
20	–30	1.40
5	45	0.90
10	45	1.12
15	45	1.25
20	45	1.15
5	–45	0.85
10	–45	1.00
15	–45	1.17
20	–45	1.40

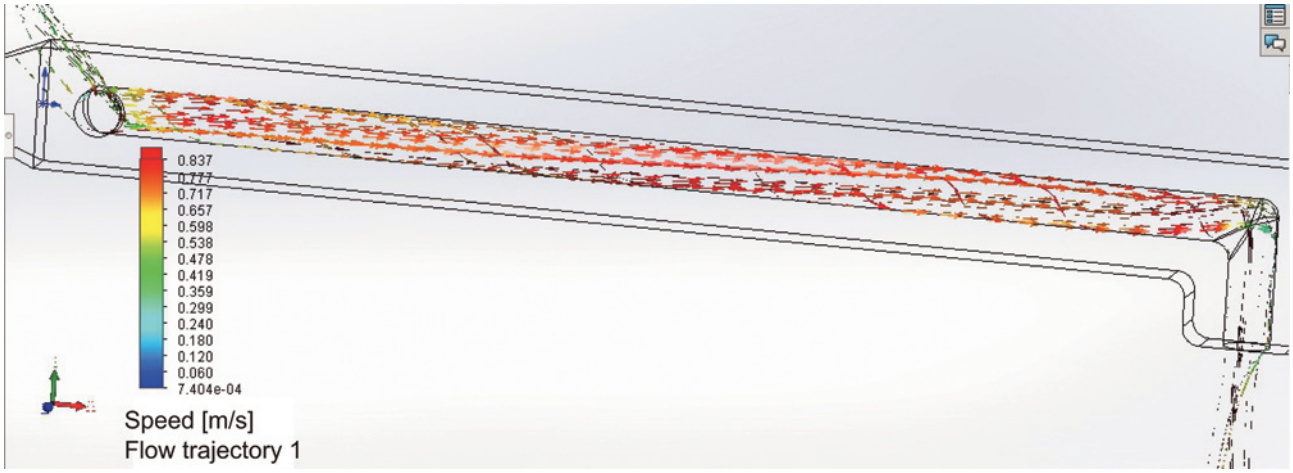

Fig. 13. A blade with a flange length of 0.05*L* bent at an angle 90°

Fig. 13. A blade with a 0.05L-long flange "knee" at an angle of 90° and the calculations of the internal airflow.

As can be noticed, the airflow has a laminar character and the velocity of 0.83 m/s. This value is several times greater than that of a straight blade design.

Increasing the flange "knee" length at a fixed angle of bending led to an increase in the airflow velocity while maintaining its laminar character. However, at greater lengths of the flange, the solar-wind turbine rotor aerodynamics and strength deteriorate. In addition, the study was conducted on how the flange angle variations effected the internal airflow velocity and its character. The optimal parameters were obtained with a flange of 0.15*L* at an angle of 30° (*Fig. 14*). The internal air flow velocity parameters can be seen in this picture as well.

In a flanged tip blade design, the internal airflow remains laminar at a speed of 1.51 m/s, which is about 8 times greater than that in a straight blade design.

A blade design with a tip flange in the opposite direction (at a negative angle) was studied and it showed a lower airflow velocity than that in the optimal design, with the airflow remaining laminar. Wherein the turbine rotational speed is reduced due to brake torque.

A blade with a deflector system

A deflector was assumed to increase the air draft in the blade internal cavity and aerodynamic resistance to rotation.

Using SolidWorks, a deflector in the form of a truncated hollow pyramid was built. An optimal blade design was chosen (see *Table 3*). The results of aerodynamic calculations for this case are shown in *Fig. 15*.

The deflector size allowed a gap spacing between the blade outside surface and the deflector inner wall.

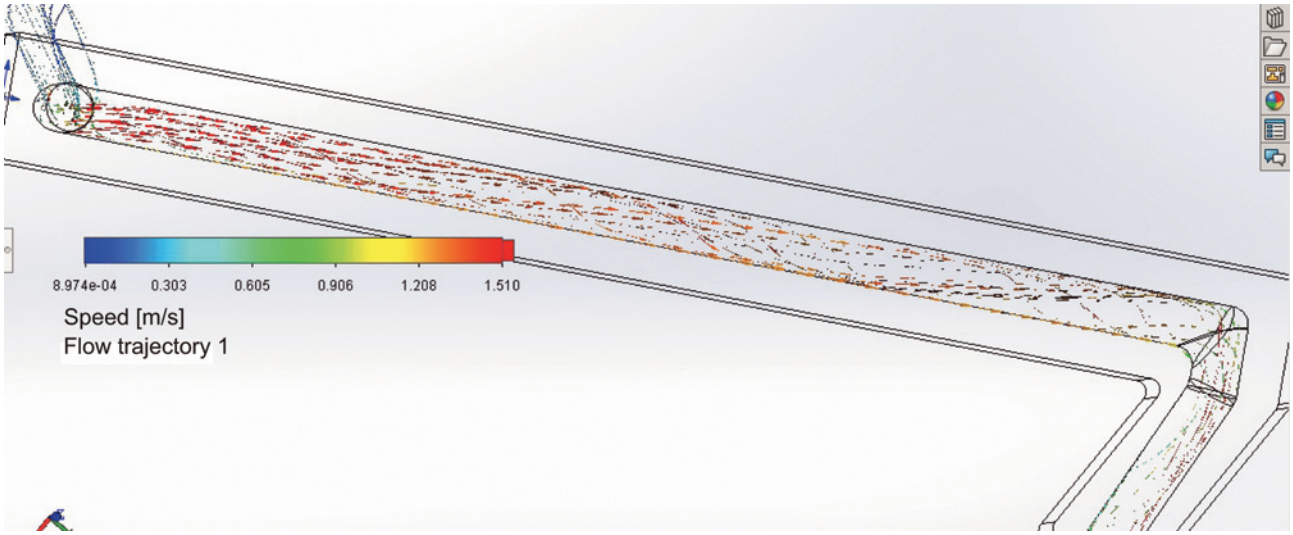

Fig. 14. Blade design and calculation results

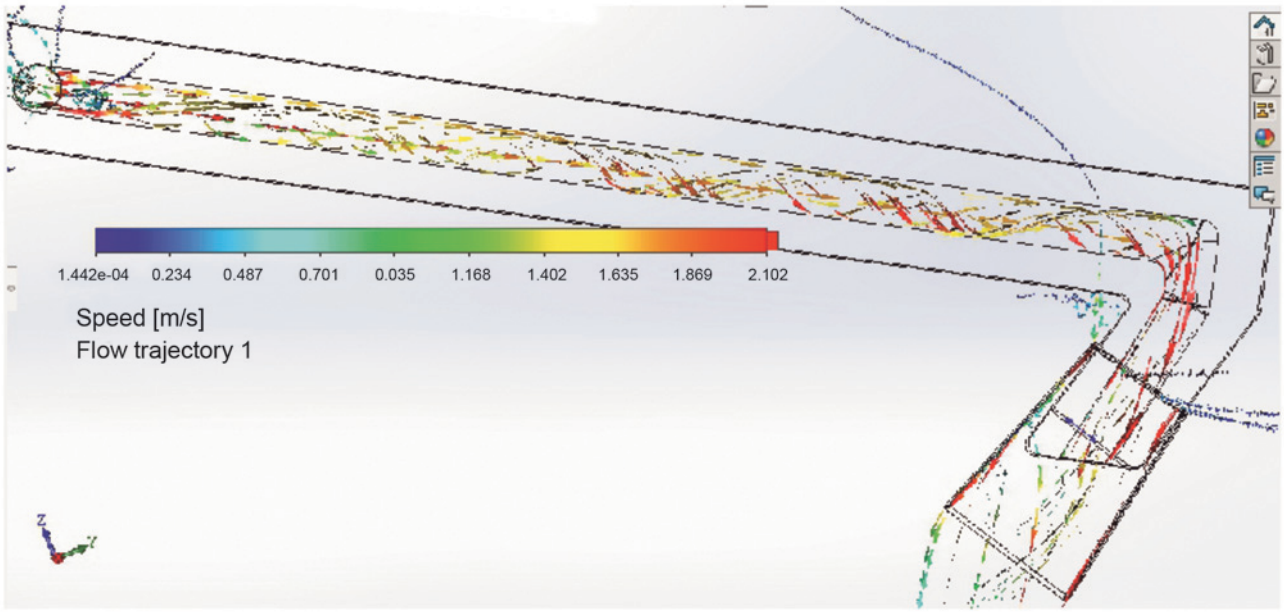

Fig. 15. Calculation results of a deflector blade

Thus, the ambient airflow rushed inside the blade tip through this gap spacing with speed acceleration. It dragged the airflow passing through the blade internal cavity along with (see *Fig. 15*).

The airflow inside the blade remained laminar.

The results showed that the airflow velocity increased 1.3 times and reached an average value of about 2 m/s.

SIMULATION OF HEAT TRANSFER FOR THE SOLAR-WIND GENERATOR BLADE USING COMSOLMULTIPHYSICS

The COMSOL Multiphysics package was used to study the effect of an airflow inside the blade on the solar panel thermal parameters.

The blades were assumed to be made of fiberglass reinforced epoxy resin of uniform thickness. The blade rotated with a constant speed of 2.62 rad/s. The sun heated the blade front surface only. Convective heat transfer was carried out only on the blade front surface. The blade back and side surfaces were thermally insulated.

The calculations were carried out for solar radiation flux of 800 W/m^2, with wind speed being 4.2 m/s and ambient air temperature being 23.8° C.

The blade inteenal cavity had the following dimensions: cavity length was 36 m, wall thickness was 0.02 m, and cross-section width was 0.2 m.

The HeatTransferinSolids interface was used for thermal calculations. Heat transfer equations (2) and (3) were used.

We can note the following regarding the boundary conditions (BC). For the upper boundary of the air flow, BC “Open Boundary” was set up, which took into account the airflow temperature equal to the ambient temperature. BC “Inflow” was used for the left boundary. It indicated the input of the airflow. BC “Outflow” was used for the right boundary and indicated the output of the airflow. BC “Heat Flux” was used to indicate the heated airflow at the blade outer boundary, and the command “Heat rate” was used to account for the flow velocity.

While setting boundary conditions, “Laminar Flow” interface was used to designate the laminar airflow parameters. The laminar air flow boundaries were set up with “Wall 1” command for the lower boundary and “Wall 2” command for its upper boundary.

The airflow velocity at the beginning of the laminar flow was set with “Inlet” command.

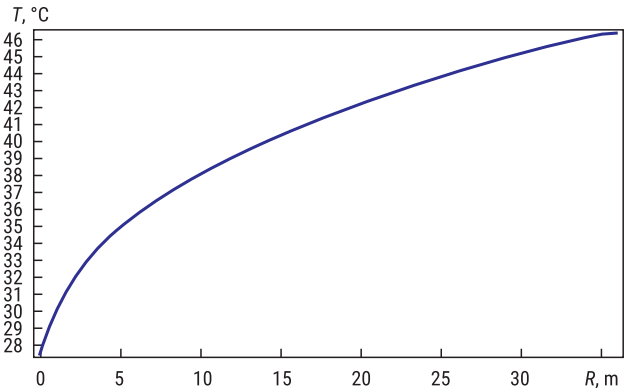

Fig. 16. Thermal calculation results

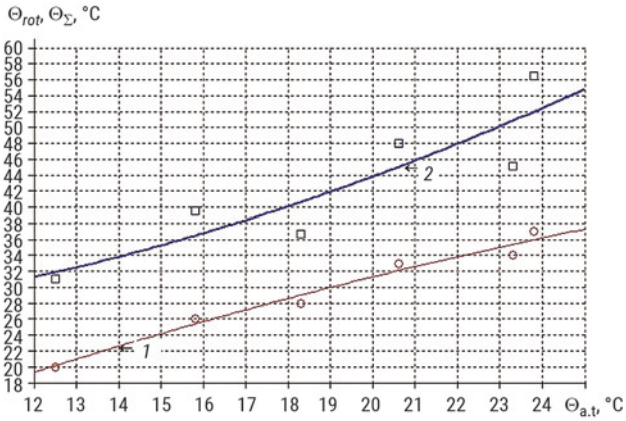

Fig. 17. Graphs show the dependence of the average blade temperature on the ambient temperature:
curve *1* is external and internal cooling; curve *2* is external cooling only; Θ_{rot} is average blade temperature resulting from blade rotation; ΘΣ is average blade temperature resulting from blade rotation and internal cooling; $\Theta_{a.t.}$ is ambient air temperature

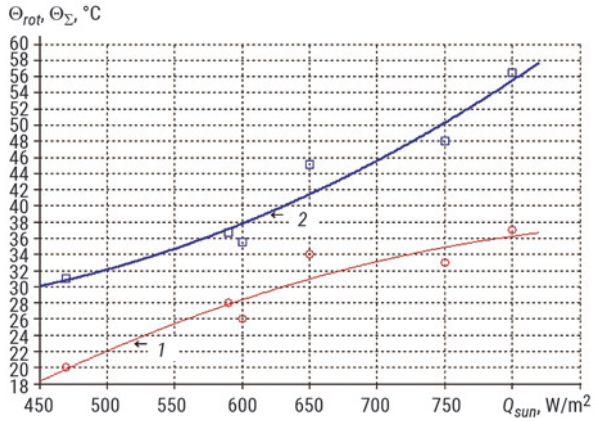

Fig. 18. Graphs show the dependence of the average blade temperature on the solar heating flux value:
curve *1* is external and internal cooling; curve *2* is external cooling only; Q_{sun} is solar heating flux

"Outlet" command was used to set up "Suppress Back flow" (pressure suppressing a backflow).

To combine two physical processes "Heat Transfer in Solids" and "Laminar flow", the "Multiphysics" command was used.

The temperature distribution along the length of the blade was obviously similar to the graph of the even-degree root. The minimum temperature of the blade wall heating was 27 °C, and the maximum temperature was about 46.5 °C. This corresponds to an average blade heating temperature of 37 °C. In this case, the steady-state temperature of the blade without internal cooling (only external cooling due to blade rotation) is equal to 56.45 °C for the specified weather conditions [7].

Therefore, the airflow passing through the blade internal cavity reduced the temperature of the blade surface by about 20° C for the considered case.

The results of thermal calculations for different weather conditions are shown in *Fig. 17*, *18*. If we compare these graphs, we can see that the blade temperature reduction due to internal cooling is in the range of 9–20 °C for the considered cases.

CONCLUSION

The optimal solar panel temperature can be effectively achieved by increasing the speed of the wind turbine rotations, which leads to an increase in the heat transfer coefficient.

At low wind speeds, it is rational to place the solar panel closer to the blade tip rather than over the entire area of the blade.

The cooling effect can be increased by using materials with less thermal resistance for solar panels and blades or by reducing their thickness.

To increase the heat transfer coefficient, it is recommended to create the airflow turbulence on the solar panel surface. This can be achieved both by changing the operational parameters and new design solutions.

To increase the solar panel cooling, it is recommended to use part of the wind flow sucked into the inner cavity of the blade. Optimizing the blade tip geometry and using deflectors will also increasethe solar panel cooling.

REFERENCES

1. Kim K.K. A variant of the vacuum transport system. *Railway Transport*. 2016;12:67-68. (In Russ.).

2. Kim K.K., Kim K.I. Suspension system of hyper loop *Transportation Systems and Technology*. 2017;3(2):9-10. DOI: 10.17816/transsyst2017329-10

3. *Certificate for utility model RU No. 24670 MKI37 B61D17/00, B61D 25/00. The body of the head car of a high-speed train*. Applicant and patent holder Emperor Alexander I St. Petersburg State Transport University; application No. 2001135610/20 12/26/2001; publ. on 04/24/20. BulletinNo. 12.

4. *Patent RU No. 197430 MKI37 F03D 9/25, H02S 10/12. Wind generator*. Applicant and patent holder Emperor Alexander I St. Petersburg State Transport University; application No. 2019139281 12/02/2019; publ. on 24/04/2020. Bulletin No. 12.

5. Gulkov V.N., Kolesnichenko I.D., Korotkov K.E. Investigation of the effect of heating solar modules on the efficiency of radiation conversion. *Proceedings of Saint Petersburg Electrotechnical University*. 2019;1:10-16. (In Russ.).

6. *Eurasian patent 040487 IPC F03D1/00, F03D9/00. Wind generator*. Applicant and patent holder Emperor Alexander I St. Petersburg State Transport University; application No. 202100092 08.26.2021; publ. on 09/06/2022.

7. Kim K., Panychev A., Blazhko L. Increasing the Efficiency of Thin-Film Silicon Solar Panels. *International Scientific Siberian Transport Forum TransSiberia – 2021*. 2022;1560-1568. DOI: 10.1007/978-3-030-96383-5_174

Bionotes

Konstantin K. Kim — Head of the Department of "Electrical Engineering and Heat Power Engineering"; **Emperor Alexander I St. Petersburg State Transport University (PGUPS)**; 9 Moskovsky pr., St. Petersburg, 190031, Russian Federation; SPIN-code: 3278-4938, ID RSCI: 690443, Scopus: 57196471944, ResearcherID: ABH-4480-2020, ORCID: 0000-0001-7282-4429; kimkk@inbox.ru;

Alexander Yu. Panychev — Rector; **Emperor Alexander I St. Petersburg State Transport University (PGUPS)**; 9 Moskovsky pr., St. Petersburg, 190031, Russian Federation; SPIN-code: 5255-1882, ID RSCI: 404314, Scopus: 57190226949, ResearcherID: G-7878-2018, ORCID: 0000-0003-1859-3097; e-mail dou@pgups.ru;

Lyudmila S. Blazhko — First Vice-Rector, Vice-Rector for Academic Affairs; **Emperor Alexander I St. Petersburg State Transport University (PGUPS)**; 9 Moskovsky pr., St. Petersburg, 190031, Russian Federation; SPIN-code: 8522-5224, ID RSCI: 275525, Scopus: 57190230361, ORCID: 0000-0001-5209-6778; blazhko@pgups.ru.

Contribution of the authors: the authors contributed equally to this article.
The authors declare no conflicts of interests.

Corresponding author: Konstantin K. Kim, kimkk@inbox.ru.

The article was submitted 01.07.2022; approved after reviewing 13.08.2022; accepted for publication 01.09.2022.